Tunable Contact Angle Hysteresis for Component Placement on Stretchable Superhydrophobic Surfaces

Catalin Mihai Balan, Alexis Vlandas, Vincent Senez

ADVANCED MATERIALS INTERFACES
www.advmatinterfaces.de

Tunable Contact Angle Hysteresis for Component Placement on Stretchable Superhydrophobic Surfaces

Catalin Mihai Balan, Alexis Vlandas, and Vincent Senez*

One of the promising strategies to achieve high performance flexible electronics is to integrate high performance components (micro-electro-mechanical systems, integrated circuit, etc.) on a flexible substrate. The heterointegration of fragile high performance components, for example, thinned down 100 GHz silicon technology, necessitate however methodologies to place these components on the substrate while exerting as little force as possible to prevent any damage from occurring. In this work, a novel approach is presented for component positioning by capillary assembly on a smart flexible substrate composed of two layers of polymers. It is shown how the wettability of the surface can be engineered by combining stretching induced deformation of the top layer with plasma treatment. Using magnetically actuated ferrofluid droplets which carry the silicon chip shows how it can be aligned and deposited at predetermined sites on these substrates. It is demonstrated that unlike standard capillary alignment which relies on a hydrophobic/hydrophilic contrast, in this case deposition is controlled by surface adhesion contrast between the site and the rest of the substrate. Furthermore, it is explained how deposition sites can be selectively activated through localized stretching thus producing generic smart substrates on which precise depositions sites can be activated according to the needs of the end user.

The wetting properties of a solid surface in contact with a liquid have a direct impact in numerous advanced technologies including flexible[1] and stretchable[2] electronics, in all application of bioinspired wettable surfaces[3,4] such as surfaces with superhydrophobicity/omniphobicity,[5–13] surfaces with patterned wettability,[14–19] integrated multifunctional surfaces and devices.[20,21] Increasingly, surface properties have been used to overcome the challenge of placing small components on flexible substrates by using, for example, adhesion[22,23] or self-assembly.[24–26] To achieve the right properties, it was soon realized that the liquid/surface interaction is not only linked to surface chemistry but is also dependent on the surface topology. Multiple length scales of roughness coupling microstructures to increase the mechanical robustness with nano texturing to retard full penetration of liquid is found in lots of natural surfaces.[5] By controlling the surface micro/nanotopology it is also possible to obtain surfaces displaying a wetting gradient or areas with distinctive wetting properties.[27,28] One way of creating geometrical patterns on surfaces is with the help of photolithography[7,8] but this has the drawback of being accomplished through expensive equipment and processes. Recently instabilities that can appear in soft materials, especially wrinkled surfaces, have been demonstrated to be a reliable and easy method to fabricate patterned surfaces.[29–33] Yang suggests strategies to control the wrinkle pattern topology and characteristic wavelength, and the recent efforts in harnessing topographic tunability in elastomeric polydimethylsiloxane (PDMS) bilayer wrinkled films in different applications are also highlighted.[34]

In this work, we present a novel approach for micro-electro-mechanical systems or integrated circuit chip positioning by capillary assembly on a smart flexible substrate composed of two layers of polymers. We show how the wettability of the surface can be engineered by combining stretching induced deformation of the top layer with plasma treatment. Using magnetically actuated ferrofluid droplets which carry the silicon chip we show how it can be aligned and deposited at predetermined sites on these substrates. We demonstrate that unlike standard capillary alignment which relies on a hydrophobic/hydrophilic contrast,[35,36] in our case deposition is controlled by surface adhesion contrast between the site and the rest of the substrate induced by a differential response to stretching of the deposition site. Furthermore, we explain how deposition sites can be stealthily embedded on a substrate and selectively activated through localized stretching thus producing generic smart substrates on which precise depositions sites can be activated according to the needs of the end user.

Flexible microstructured substrates with 16 deposition sites were fabricated from PDMS using a silicon mold. The fabrication of the mold was done by photolithography with the use of two photolithographic masks; one for the pillars

Dr. C. M. Balan,[+] Dr. A. Vlandas, Dr. V. Senez
BioMEMS, Univ. Lille, CNRS, ISEN
UMR 8520 – IEMN, F-59000 Lille, France
E-mail: alexis.vlandas@iemn.univ-lille1.fr
Dr. C. M. Balan
National Oceanography Centre Southampton
Ocean Technology and Engineering Group
University of Southampton Waterfront Campus
European Way, SO14 3ZH Southampton, UK
The ORCID identification number(s) for the author(s) of this article can be found under https://doi.org/10.1002/admi.201701353.
[+]Present address: National Oceanography Centre Southampton, Ocean Technology and Engineering Group, University of Southampton Waterfront Campus, European Way, SO14 3ZH Southampton, UK

DOI: 10.1002/admi.201701353

and one for the deposition sites. No alignment was imposed between the two masks, consequently no preferential orientation of the deposition sites relative to the pillars structure is present. The PDMS was spin-coated and films of 50 μm thickness were obtained. Those were peeled off and placed on Pyrex glass wafers (with thickness of 0.5 mm) to ensure an adequate mechanical support when the experiments were performed. Small silicon parts (2×2 mm^2) are produced from 3 in. silicon wafers which were precut and then thinned down to 100 μm by a chemical mechanical planarization method. The parts were manually placed with tweezers on the ferrofluid droplets. The magnetic fluids were water-based and were produced in-house (the fabrication procedure and the fluid properties are provided in the Experimental Section). A permanent magnet was mounted on the moving stage of a syringe pump (KD Scientific, USA). The linear motion of the syringe pump can be programmable, and therefore the velocity of the permanent magnet was controlled and maintained constant. In all the experiment a constant velocity of ≈0.4 mm s^{-1} was maintained. The magnet was in a direct contact with the glass wafer on which the PDMS substrate sits. Videos of the droplet and its silicon payload motion were acquired at 100 fps with a microscopic magnification of 10× objective attached to a fast complementary metal–oxide–semiconductor camera (Phantom Miro M310). From the acquired videos picture were extracted at different time intervals.

Figure 1 shows a schematic illustration of the proposed self-positioning method of small silicon parts on structured substrates with premade deposition sites. Depending on the sequence of steps used in the fabrication process of the flexible substrates (which will be discussed further in the paper) the deposition sites can be set in a high or low adhesion state while remaining hydrophobic. A high receding contact angle (RCA) on the deposition site will not enable a self-placement of the silicon parts (low adhesion, Figure 1a), in contrast with a zero RCA (high adhesion, Figure 1b), which will make the silicon parts to deposit on the sites.

We prepared three different types of superhydrophobic flexible substrates for testing. The fabrication process for each one is presented in **Figure 2**. Depending on the steps sequence adopted in the fabrication process the deposition sites are either active (the self-positioning will appear, Figure 2a,c) or are in a "stealth mode" and the silicon parts will not be deposited, as seen in Figure 2b. Regardless of the surface properties, the PDMS film is peeled off from the silicon mold and thereafter coated with a thin layer of parylene-C (≈3 μm) grown by a vapor polymerization deposition (VPD) method (described in the Experimental Section). The porous nature of the PDMS enables parylene-C monomers to diffuse into the bulk polymer,[37,38] which results in a strong adhesion between these two polymer layers. Consequently, the composite bilayer substrate can be manually stretched and no delamination will appear at the bonding interface. Due to the difference in the material properties, PDMS being an elastic material and parylene which is more plastic, a stretching step will induce instabilities in the composite bilayer which produces wrinkles on the parylene layer surface.[39] Because of the random manual stretching, without a sequential loading procedure or a predictive design, the wrinkles are formed with no ordered topologies. Nevertheless, the wrinkles can be seen forming on the bottom surface around the pillars' bases, and on top of the deposition sites (see scanning electron microscopy (SEM) images in Figure 2). No wrinkles will form on the top of the pillars due to their high aspect ratio ($AR = h/a$), defined as the ratio between the height of the pillar h and the length a, as sketched in Figure 1 which prevent efficient transfer of the stretching forces from their base to their top surface.

To increase the hydrophobicity of the surface a plasma surface treatment approach was employed. The plasma treatment is required to make the substrate suitable for magnetic actuation as without it, maintaining the droplet in a nonimpaled Cassie–Baxter state when the permanent magnet is brought into working position is not possible. The adopted treatment combines oxygen (O_2) plasma pretreatment with a sulfur

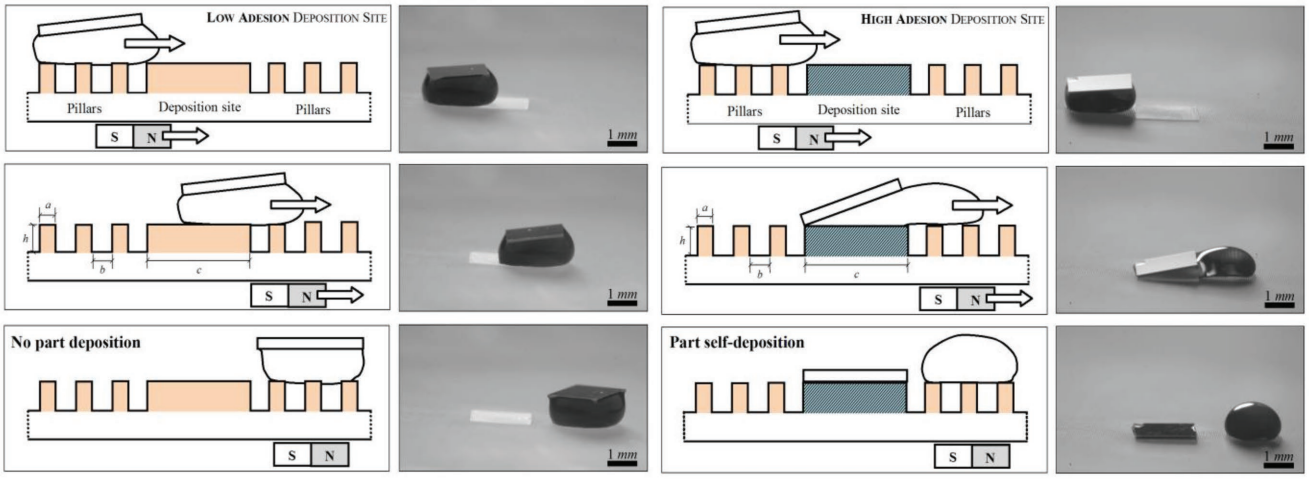

Figure 1. Schematics of the ferrofluid droplet carrying a silicon part and its actuation by a permanent magnet. The displacement is performed on superhydrophobic structured substrates with pillar regions (side (a) of 20 μm and height (h) of 50 μm) and deposition sites. The deposition sites are square shaped with the same length side (c) 2 mm as the silicon parts and are either in a low or high adhesion state. On the left side images show a low adhesion deposition site for which no part deposition takes place as the receding contact angle is ≈130°. The images from the right side show the case when the part is deposited on the substrate due to a 0° receding contact angle.

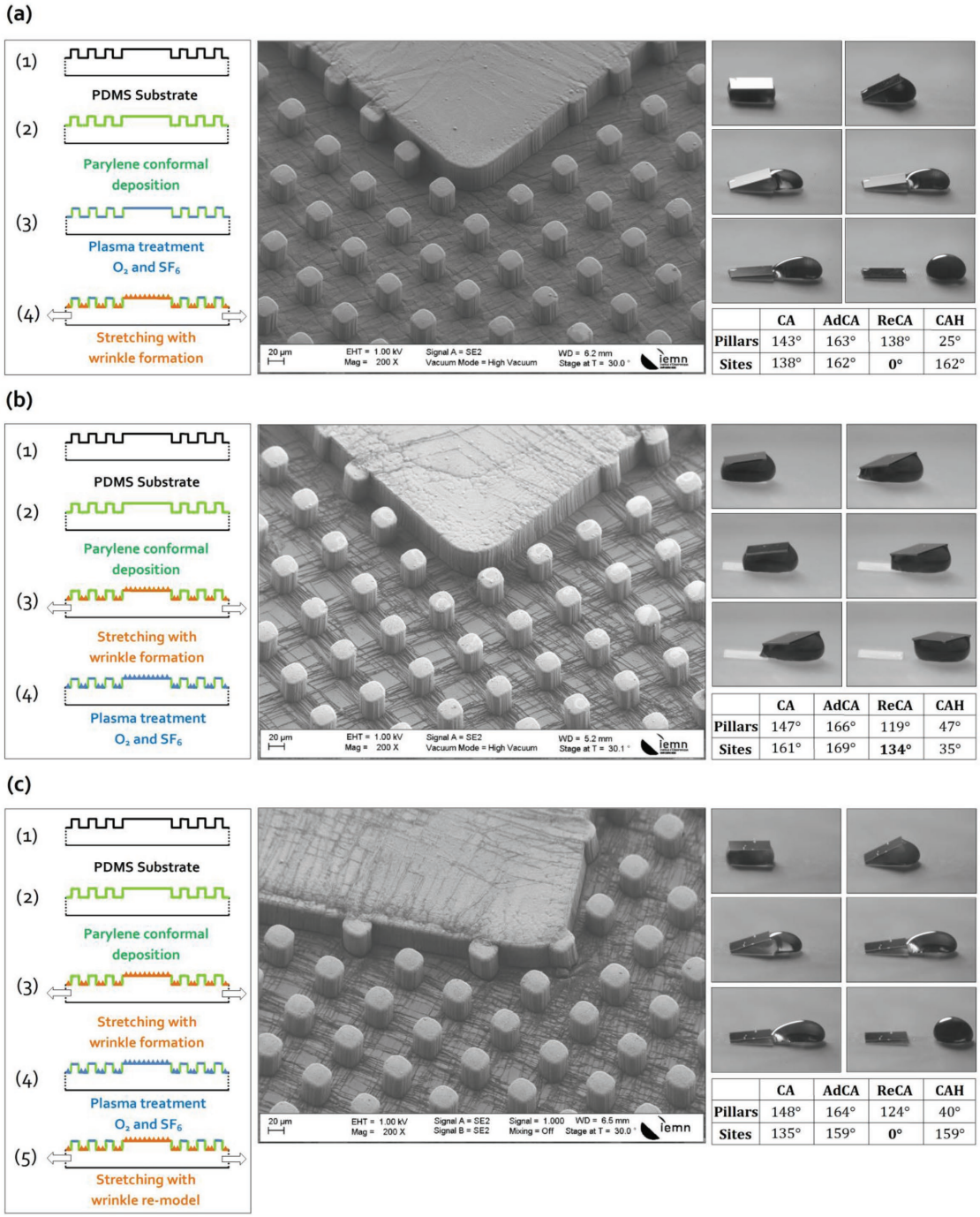

Figure 2. Substrates having experienced three sequences of fabrication steps (schematics shown left) are tested for part self-assembly. a–c) In all cases, the PDMS substrates are covered with a conformal parylene layer of ≈3 µm and are plasma treated. (a) The plasma treatment followed by a mechanical stretching of the entire substrate will transform the pillar regions in low adhesion ones and the deposition sites in high adhesion one, allowing the parts to be deposited. (b) The switching between step 4 and 3 in the fabrication process, will transform not only the region with pillars in low adhesion ones but also the deposition sites, putting them in a stealth configuration. (c) By performing a second stretching locally or over the entire substrate the deposition sites are activated so that the placement of the parts will take place. All CA measurements are performed at the end of the production process.

hexafluoride (SF_6) plasma treatment as proposed by Bi[39,40] for the modification of surface wettability on the parylene-C films. The O_2 plasma pretreatment is used to create the nanoscale features on the surface. It will however also raise the surface free energy due to the creation of carbonyl (C=O) and carbonate groups (O_2C=O)[40] resulting in an improved wettability. The subsequent SF_6 plasma will help lowering the surface energy by adding fluorinated groups and thus contribute to the hydrophobic behavior. As a result we achieve superhydrophobicity on the pillars regions by having dual length scale texturing with

nanoscale features on top of the pillars (which are representing the microscale) thus preventing droplet impalement while not altering the PDMS bulk properties (e.g., mechanical properties).

We will now explain how the interplay between the two steps in the fabrication process, mechanical stretching and the plasma treatment, influences the dynamical wetting properties of the deposition sites' surface. We can do so by comparing Figure 2a and b in which we perform the plasma step either before or after stretching. In both cases, the pillar regions of the substrate are robust to impalement (CA > 140°) and have low hysteresis. Regardless of the order as well, wrinkles are formed on top of the deposition sites and the static wetting properties are minimally impacted with CA > 138. The dynamical wetting properties however vary greatly, with the RCA measured on the sites being strongly impacted by the order in which these two steps take place.

Indeed, if the mechanical stretching step is performed last as in Figure 2a, we measure a low RCA and a high hysteresis (162°) which leads to a very efficient part deposition. The strong triple line pinning associated with the high hysteresis at the deposition site is in the view due to re-exposure of carbonyl groups (C=O) and carbonate groups (O_2C=O) produced by the O_2 plasma step.[39] As described in **Figure 3**a, stretching the plasma treated parylene surface to produce wrinkles introduces breaks in the SF6-treated top layer thus exposing oxygen rich domains. As a result, all the sites of this substrate are always activated for part self-placement.

Conversely, when the plasma step is done last as in Figure 2b, the deposition sites inherit wetting properties that will make them nonactive for a silicon part self-placement. The deposition sites display low wetting behavior (CA = 167°), the RCA is high (138°), and the hysteresis is low (35°). This can be explained simply by the dual scale induced hydrophobicity at their surface. Indeed, the wrinkle topography produced by mechanical stretching of the composite PDMS/parylene bilayer (which represents the microscale), combined with the employed plasma treatment (which creates the nanoscale) results in a very robust hydrophobic surface.

Finally, we study the effect of a second mechanical stretching applied to the surfaces from Figure 2b. Interestingly, this step transforms the wrinkled deposition sites from low adhesion to high adhesion making them suitable for part deposition (Figure 2c). The origin for this effect is similar to the pining effect discussed above and described in Figure 3a even though the wrinkles have already been formed by the first stretching step. Indeed, while SEM characterization of the top of the deposition sites before and after the second mechanical stretching shows no important changes in the wrinkle topography (Figure 3b), one can see that the ridges at the apex of the wrinkle appear to be cracked open. We believe that these regions expose—once again—oxygen rich surfaces which tend to increase the hysteresis. The X-ray photoelectron spectroscopy (XPS) analysis (shown in **Table 1**) conducted prior and after stretching confirms that the ratio of oxygen to fluorine in the topmost nanometers of our surface is indeed strongly affected by the stretching step with the ratio O/F going from 0.28 to 40 which comforts this explanation.

This switching of wetting hysteresis by mechanical stretching is interesting as it can be performed on the whole substrate at once or locally on individual sites. By doing the latter, it is possible to put some designated deposition sites in an "active mode" which permits deposition while leaving the others in a "stealthy mode."

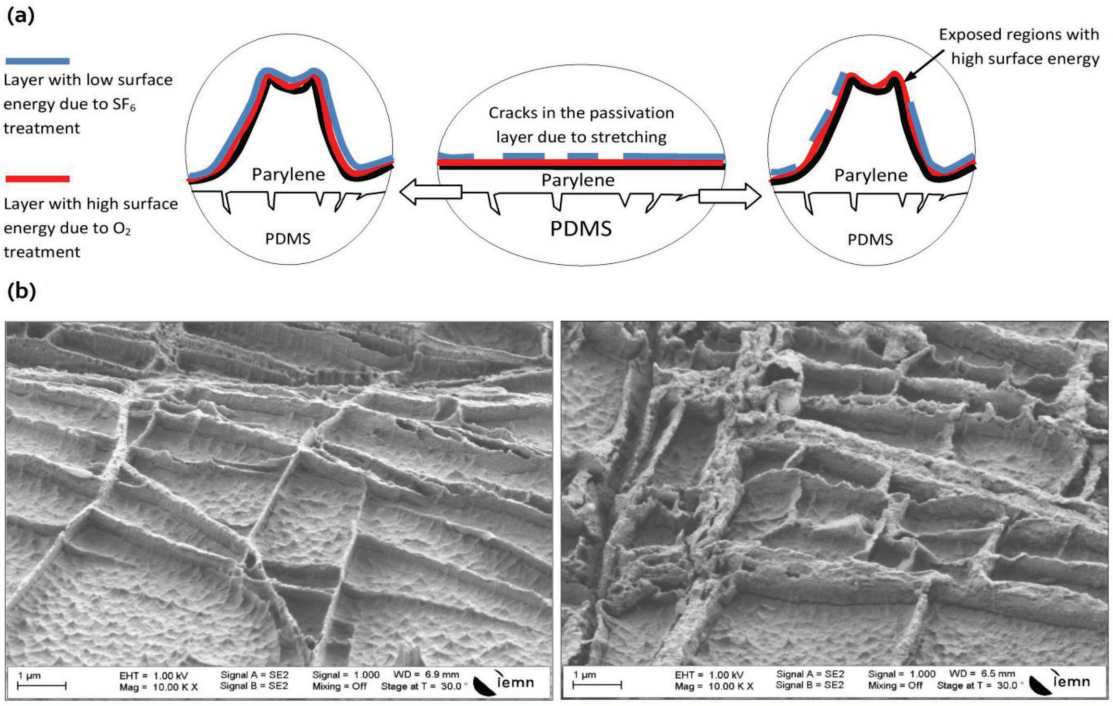

Figure 3. a) Schematic illustration with the wrinkles formed on the deposition sites and the transformation process from low surface energy into a high energy surfaces by mechanical stretching. b) SEM pictures of substrates before and after stretching showing how the second stretching step break open the top of the wrinkles.

Table 1. XPS analysis of the surface before and after the stretching step.

XPS edge	O1s		C1s		F1s	
	Binding energy [eV]	Peak area	Binding energy [eV]	Peak area	Binding energy [eV]	Peak area
Nonstretched	534,6	4182	287	9770	690,5	14715
Stretched	533,35	11470	285,1	9325	688,2	285

We evaluated the placement precision and reproducibility for substrates which had gone through the production process described in Figure 2a,c (as no deposition occurs in Figure 2b). The substrates were designed with 16 deposition sites as sketched in **Figure 4**a and the statistics are shown in Figure 4b. The evaluation process was performed as follows: first the silicon parts were consecutively placed on a magnetic droplet manually with tweezers, then the magnetic droplet was moved across the flexible substrate and the deposition sites following the constant movement of a permanent magnet. Optical pictures of each deposited part were acquired by a CCD camera via a 2× magnification microscope objective. Each site was tested five times following the same protocol of self-placement and image acquisition. Between each deposition evaluation the silicon parts were detached from the deposition sites with deionized water, recovered and then washed and sonicated in isopropanol and let it dry over a few hours in a clean Petri dish.

Figure 4a (left side) presents a sketch of the parameters measured when evaluating a silicon part deposited on a site: the angle orientation of the silicon part relative to the deposition site (α) and the distance between the two centers (δ). The displacement distance X can be defined as

$$X = \delta + \frac{a\sqrt{2}}{2} \cdot \cos\left(\frac{\pi}{4} - \alpha\right) \tag{1}$$

with a being the length of the silicon part.

All variables such as angle (α) and distances (δ and L the length of the deposition site) were measured from the optical pictures acquired after each deposition using ImageJ.[41] Due to mechanical stretching of the PDMS substrates conducted under wet condition in isopropanol, and then placement on glass wafers to provide mechanical support, the deposition sites are slightly bigger than the silicon parts themselves. From

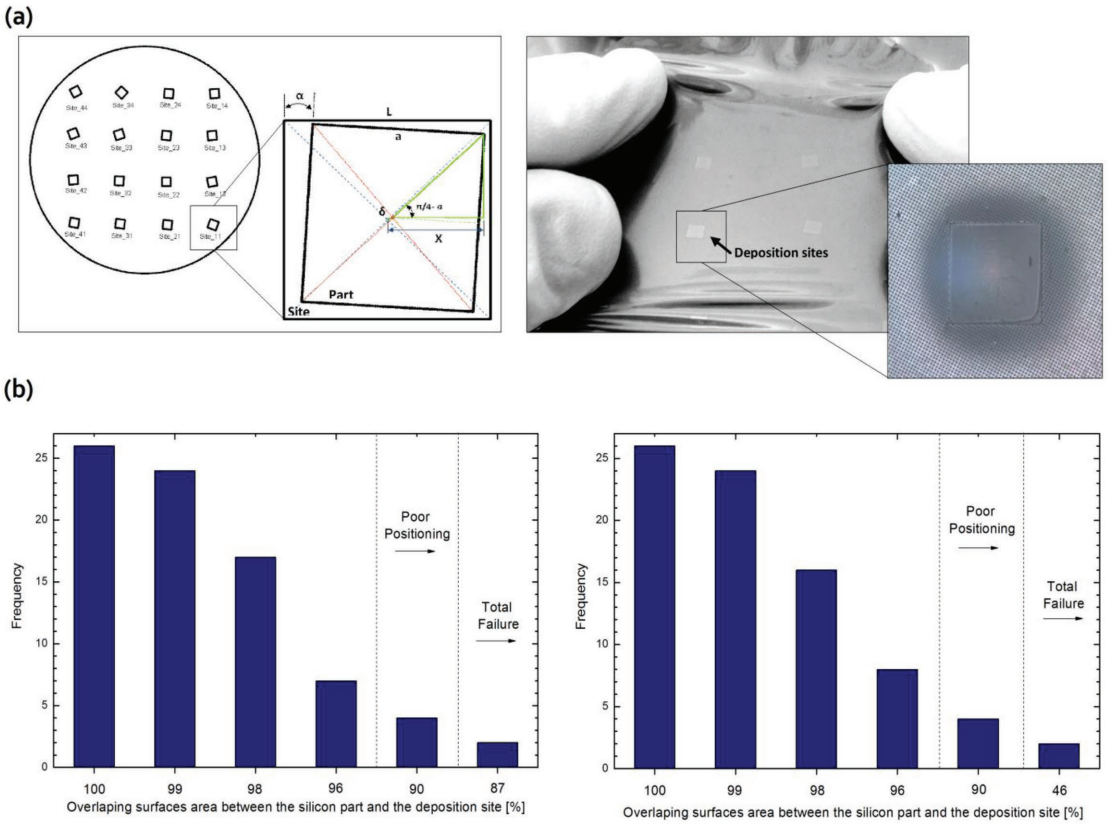

Figure 4. a) Schematic illustration with the deposition sites and the evaluation criteria of the parts deposition is given in the left side. The angle orientation of the silicon part relative to the deposition site α and the distance between the two centers δ. On the left, a photograph of the stretching process and in inset a deposition site. b) The statistical evaluation over 80 trials on the self-placement process is quantified in graphical representations. The left side shows the results for the always activated substrate and the right side the deposition results for the stretched stealth substrate.

the acquired images the area was estimated to be >5% greater than the nominal value. The depositions were evaluated by binning the attempts as a function of their area overlap value. An overlap of less than 96% was considered as a poor part deposition and one of less than 90% to be a failure. This tends to happen only when regions similar in surface area to the silicon parts are losing the Cassie–Baxter state near the deposition sites due to surface contamination or defects. Figure 4b presents the 80 self-deposition evaluations conducted. These statistics show that the proposed part self-deposition approach is reliable, with more than 91% of the parts assembled properly and just two parts for each substrate failing to sit on the designated deposition site. Also we can conclude that "stealth sites" are as effective at positioning parts once activated as the sites which are always active (produced according to Figure 2a).

In summary, we have presented a novel way to control deposition and alignment of small silicon parts on a flexible and stretchable substrate. We do so by relying on ferrofluid droplets to act as a conveyor belt and by controlling the dynamical wetting properties of the surface. This method has proved to be a robust one, with more than 91% of the parts assembled correctly. The use of a magnetic field as a noncontact actuation mechanism makes it possible to foresee easy automation of placement through the use of an electromagnets array for example. Another novelty of the present paper is the proposed fabrication method of the flexible substrates, composed of two layers of polymer PDMS and parylene, and the possibility to switch by a simple mechanical stretching action the deposition sites from a "stealth" state for which no part deposition takes place to an active one. With this we envision of a new approach in smart-placement procedures, by creating a mass produced master template that can be embedded in the substrate, and different assembly configuration can be achieved on these smart flexible substrates by a simple local stretching approach.

Experimental Section

Silicon Mold Fabrication: Photolithography was employed to obtain the silicon molds from which the PDMS substrates were created. The needed patterns were designed by using AZ 9260 positive resist and two photolithographic masks. The first mask which is containing the features of the pillars is a printed plastic mask, and the second mask used for the creation of the deposition site is a shadow mask fabricated in house from a Pyrex glass wafer covered with a 100 nm of chromium. To open the windows in the shadow mask 16 silicon parts were placed relatively random on the silicon wafer after negative photoresist was spin-coated. The exposure and baking of the photoresist was followed by the windows opening in developer by removing the nonexposed photoresist but also the underneath chromium. After the two exposures, the AZ 9260 photoresist was baked and developed. The substrate was then etched vertically (≈50 µm) using the Bosch process on an ICP system (STS Multiplex IPC etch).

Preparation of PDMS Structured Substrates: The Sylgard 184 Silicon elastomer Kit from Dow Corning was used for the preparation of the PDMS thin films. The elastomer and the curing agent were mixed at a ratio of 10:1. After a proper degasification under vacuum to remove the air bubbles, the PDMS was carefully poured on the silicon mold until the all wafer surface was covered. The PDMS was spin-coated at 1500 rpm for 60 s, and placed on a hot plate for 10 min at 150 °C for the curing process. The cross-shaped PDMS films, ≈50 µm, were gently peeled off from the silicon mold in isopropanol wet condition. The flexible substrate was then placed on glass wafers and let them rest for 24 h in ambient atmosphere, for the isopropanol to evaporate.

Parylene Conformal Deposition: 3 µm thick parylene-C films were prepared through VPD method, using a compact parylene treatment machine C 20S (Comelec, Swiss). During this process, the raw material dimer dichloro-di(p-xylylene) it was first vaporized at 150 °C under vacuum and then pyrolyzed at 690 °C to generate the monomeric form chloro-p-xylylene. The monomer subsequently condenses at room temperature onto the PDMS structured substrates in the deposition chamber to form conformal parylene-C thin films. The thickness of the parylene-C films was dependent by the amount of the initial loading dimer and verified by a profilometer (DektakXT, Bruker).

Surface Plasma Treatment: The plasma treatment was performed in a reactive ion etching system (Plasmalab 80 Oxford Instruments, United Kingdom) using O_2 plasma followed by SF_6 plasma. The experimental has been performed at a chamber pressure of 20 mT, under a constant flow rate of 50 sccm. The plasma was ignited at a fixed radio-frequency power of 100 W. The O_2 plasma treatment of parylene-C was carried out for 7 min and 30 s, and after that SF6 plasma was applied to the substrates for 2 min.

Magnetic Fluid Preparation: The synthesis of the magnetic fluids was conducted in the chemistry room of IEMN institute, and is based on the reaction of iron(II) and iron(III) ions in an aqueous ammonia solution to form magnetite, Fe_3O_4 as shown below[42]

$$2FeCl_3 + FeCl_2 + 8NH_3 + 4H_2O \rightarrow Fe_3O_4 + 8NH_4Cl \quad (2)$$

The magnetite was then mixed with aqueous tetramethylammonium hydroxide, $(CH_3)4NOH$, solution. The magnetite particles were surrounded by this surfactant with hydroxide anions and tetramethylammonium cations to create an electrostatic interparticle repulsion in an aqueous environment.[43] As a last step, the concentration of the magnetic fluid was adjusted by a strong centrifugation of the sample (10 000 rpm for 10 min).

Contact Angle Measurements: The contact angles were measured with the magnetic fluid employed in the experiments using a contact angle analyzer (Drop Shape Analyzer DSA 100, Kruss, Germany). Dynamic advancing and receding CAs were recorded while the magnetic fluid was added to and withdrawn from the drop, respectively, by the injection mechanism of the equipment. The measurements were effectuated on all structured substrates, and for the site wetting characterization flat surfaces were produced and employed. The flat surfaces were fabricated using the same protocol as for the structured ones. For each sample typical error in measurement was ≈2°.

Surface Characterization: The surface wrinkles morphology and geometry were studied using a Zeiss SEM. The characterizations was conducted on an extra PDMS surface that was covered with 3 µm of parylene and cut in small samples each one containing two deposition sites. The samples were then placed on a silicon wafer and engineered following the same protocols as in the main experiments. In the end the wettability behavior was also checked to have the same behavior. Prior SEM characterization the samples were covered with 20 nm of Au to avoid charging effects. The XPS experiments were carried out using Al Kα ($h\upsilon$=1486.6 eV) radiation from a monochromatic X-ray source and a hemispherical energy analyzer. The collection angle was set at 45° and the analyzer pass energy was set at 11.75 eV. Furthermore, due to charging up of the surface, the samples were neutralized using either 5 V/17.9 or 8 V/19 mA condition. The spectra were thereafter realigned using the carbon edge at 285 eV and the area under the various peak integrated for elemental ratio quantification.

Supporting Information

Supporting Information is available from the Wiley Online Library or from the author.

Acknowledgements

This work was supported in part by the French Government through the National Research Agency (ANR) under program PIA EQUIPEX LEAF (ANR-11-EQPX-0025). The authors would also like to acknowledge the support of the RENATCH network. C.M.B, A.V., and V.S. wish to thank J.-L. Codron at IEMN for XPS data acquisition.

Conflict of Interest

The authors declare no conflict of interest.

Keywords

capillary self-placement, dynamic wettability, magnetic actuation, smart surfaces, stretchable superhydrophobic surfaces

Received: October 19, 2017
Revised: February 10, 2018
Published online: April 3, 2018

[1] S. Lee, W. Kim, K. Yong, *Adv. Mater.* **2011**, *23*, 4398.
[2] J. Park, S. Wang, M. Li, C. Ahn, J. K. Hyun, D. S. Kim, D. S. Kim, D. K. Kim, J. A. Rogers, Y. Huang, S. Jeon, *Nat. Commun.* **2012**, *3*, 916.
[3] X. Yao, Y. Song, L. Jiang, *Adv. Mater.* **2011**, *23*, 719.
[4] K. Liu, Y. Tian, L. Jiang, *Prog. Mater. Sci.* **2013**, *58*, 503.
[5] M. Sun, C. Luo, L. Xu, H. Ji, Q. Quyang, D. Yu, Y. Chen, *Langmuir* **2005**, *21*, 8978.
[6] B. Cortese, S. D'Amone, M. Manca, I. Viola, R. Cingolani, G. Gigli, *Langmuir* **2008**, *24*, 2712.
[7] K. Tsougeni, A. Tserepi, G. Boulousis, V. Constantoudis, E. Gogolides, *Plasma Processes Polym.* **2007**, *4*, 398.
[8] A. Tropmann, L. Tanguy, P. Koltay, R. Zengerle, L. Riegger, *Langmuir* **2012**, *28*, 8292.
[9] Z. Chu, S. Seeger, *Chem. Soc. Rev.* **2014**, *43*, 2784.
[10] E. Celia, T. Darmanin, E. Taffin de Givenchy, S. Amigoni, F. Guittard, *J. Colloid Interface Sci.* **2013**, *402*, 1.
[11] W. Wang, J. Salazar, H. Vahabi, A. Joshi-Imre, W. E. Voit, A. K. Kota, *Adv Mater.* **2017**, *29*, 1700295.
[12] R. Hensel, C. Neinhuis, C. Werner, *Chem. Soc. Rev.* **2016**, *45*, 323.
[13] S. Pan, A. K. Kota, J. M. Mabry, A. Tuteja, *J. Am. Chem. Soc.* **2013**, *135*, 578.
[14] A. R. Parker, C. R. Lawrence, *Nature* **2001**, *414*, 33.
[15] C. M. Chen, S. Yang, *Adv. Mater.* **2013**, *26*, 1283.
[16] J. Li, X. Tian, A. P. Perros, S. Franssila, V. Jokinen, *Adv. Mater. Interfaces* **2014**, *1*, 1400001.
[17] T. Neckernuss, S. Wiedemann, A. Plettl, P. Ziemann, *Adv. Mater. Interfaces* **2014**, *1*, 1300033.
[18] S. M. Kang, C. Lee, H. N. Kim, B. J. Lee, J. E. Lee, M. K. Kwak, K. Y. Suh, *Adv. Mater.* **2013**, *25*, 5756.
[19] C. Y. Hang, M. F. Lai, W. L. Liu, Z. H. Wei, *Adv. Funct. Mater.* **2015**, *25*, 2670.
[20] L. Feng, Z. Y. Zang, Z. H. Mai, Y. M. Ma, B. Q. Liu, L. Jiang, D. B. Zhu, *Angew. Chem., Int. Ed.* **2004**, *43*, 2012.
[21] X. C. Gui, J. Q. Wei, K. L. Wang, A. Y. Cao, H. W. Zhu, Y. Jia, Q. K. Shu, D. H. Wu, *Adv. Mater.* **2010**, *22*, 617.
[22] M. A. Meitl, Z. T. Zhu, V. Kumar, K. J. Lee, X. Feng, Y. Y. Huang, I. Adesida, R. G. Nuzzo, J. A. Rogers, *Nat. Mater.* **2006**, *5*, 33.
[23] R. Dufour, P. Brunet, M. Harnois, R. Boukherroub, V. Thomy, V. Senez, *Small* **2012**, *23*, 1229.
[24] S. A. Stauth, B. A. Parviz, *Proc. Natl. Acad. Sci. USA* **2006**, *28*, 13922.
[25] U. Srinivasan, D. Liepmann, R. T. Howe, *J. Microelectromech. Syst.* **2001**, *1*, 17.
[26] M. Mastrangeli, W. Ruythooren, J. P. Celis, C. V. Hoof, *IEEE Trans. Compon., Packag., Manuf. Technol.* **2011**, *1*, 133.
[27] R. Holmes, K. F. Böhringer, *Microsys. Nanoeng.* **2015**, *1*, 15022.
[28] J. B. Brzoska, F. Brochard-Wyart, F. Rondelez, *Langmuir* **1993**, *9*, 2220.
[29] E. Cerda, L. Mahadevan, *Phys. Rev. Lett.* **2003**, *90*, 074302.
[30] Y. C. Chen, A. J. Crosby, *Adv. Mater.* **2014**, *26*, 5626.
[31] A. Auguste, L. Jin, Z. Suo, R. C. Hayward, *Soft Matter* **2014**, *10*, 6520.
[32] C. M. Stafford, C. Harrison, K. L. Beers, A. Karim, E. J. Amis, M. R. Vanlandingham, H. C. Kim, W. Volksen, R. D. Miller, E. E. Simonyi, *Nat. Mater.* **2004**, *3*, 545.
[33] A. Schweikart, A. Fery, *Microchim. Acta* **2009**, *165*, 249.
[34] S. Yang, K. Khare, P. C. Lin, *Adv. Funct. Mater.* **2010**, *20*, 2550.
[35] B. Chang, A. Shah, Q. Zhou, R. H. A. Ras, K. Hjort, *Sci. Rep.* **2015**, *5*, 14966.
[36] Y. Ding, L. Hong, B. Nie, K. S. Lam, T. Pan, *Lab Chip* **2011**, *11*, 1464.
[37] Y. Chen, W. Pei, R. Tang, S. Chen, H. Chen, *Sens. Actuators, A* **2013**, *189*, 143.
[38] M. W. Toepke, D. J. Beebe, *Lab Chip* **2006**, *6*, 1484.
[39] A. Takei, L. Jim, H. Fujita, *Appl. Mater. Interfaces* **2016**, *8*, 24230.
[40] X. P. Bi, N. L. Ward, B. P. Crum, W. Li, *Plasma-treated switchable wettability of parylene-C surface*, 2012 7th IEEE International Conference on Nano/Micro Engineered and Molecular Systems (NEMS), Kyoto **2012**, pp. 222–225, https://doi.org/10.1109/NEMS.2012.6196761.
[41] C. A. Schneider, W. S. Rasband, K. W. Eliceiri, *Nat. Methods* **2012**, *9*, 671.
[42] X. P. Bi, B. P. Crum, W. Li, *J. Microelectromech. Syst.* **2014**, *3*, 222.
[43] P. Jolivet, N. B. Adelman, K. J. Beckman, D. J. Campbell, A. B. Ellis, J. M. Fruchart, G. C. Lisensky, *J. Chem. Ed.* **1999**, *76*, 943.